Draft version November 6, 2018
Typeset using LaTeX default style in AASTeX62

HERA memo 56: Current status and understanding of bispectrum phase approach to detect HI from Cosmic Reionization

Nithyanandan Thyagarajan,[1] Chris Carilli,[1,2] Bojan Nikolic,[2] James Kent,[2] Kingsley Gale-Sides,[2] Siyanda Matika,[3,4] Gianni Bernardi,[3,4,5] and The HERA Collaboration

[1] *National Radio Astronomy Observatory*
1003 Lopezville Road
Socorro, NM 87801, USA
[2] *University of Cambridge, Cambridge, UK*
[3] *Rhodes University, South Africa*
[4] *Square Kilometre Array South Africa*
[5] *INAF-IRA, Italy*

ABSTRACT

Recently, a new approach to detecting HI from the Epoch of Reionization (EoR) using bispectrum phase was introduced, which will be immune to antenna-based systematics in an interferometric measurement of the brightness temperature fluctuations of redshifted HI. This primarily includes antenna-based gains that corrupt the wavefront due to the ionosphere as well as due to instrumental effects. If not accounted for at a very high precision ($\sim$ 1 part in 100,000), these uncertainties, especially along the frequency axis, will potentially render the cosmological HI signal undetectable. The bispectrum phase, however, is unaffected by these antenna-based gains and their uncertainties. Here, we discuss the connection of this approach to the prevalent power spectrum approach. Initial results from $\sim$ 40 min of HERA IDR 2.1 data around the transit of Fornax A are very promising, with a noise-limited dynamic range of $\sim 10^{7.5}$–10^8 achieved between the foreground-dominated ($k_\parallel \lesssim 0.1\,h$ Mpc^{-1}) and the larger ($k_\parallel \gtrsim 1\,h$ Mpc^{-1}) spatial modes where the reionization HI signal is expected to dominate. Power at $\tau = \pm 1\,\mu$s from the 150 m cables are prominent but are able to be mitigated down to a factor of $\sim 10^7$ relative to the power spectrum peak. This dynamic range of 10^8 is interesting because modeling seems to suggest that EoR signals stronger than a fiducial model can become separable from foregrounds and noise at this dynamic range. We are currently undertaking modeling efforts to gain a better understanding of the relative contributions of the foregrounds, EoR HI signal, and noise components in our results and the correspondence to standard power spectrum results. We will then apply the analysis to the full data set from last winter, include more classes of triads, and include both RFI-frequency ranges indentified in memo 54.

1. INTERPRETATION AND CONNECTION TO A STANDARD POWER SPECTRUM

Thyagarajan et al. (2018) have shown the potential for using interferometric bispectrum phase (aka closure phase) to detect the EoR signal using a power spectrum methodology very similar to the delay spectrum approach. Numerous references cited therein such as Carilli et al. (2018) and other memos (Carilli & Sims 2016; Carilli & Nikolic 2017; Kent et al. 2018) have elaborated on why the bispectrum phase is impervious to antenna-based gains, and therefore, their calibration and the uncertainties. This will eliminate potentially a major source of systematic that is believed to be affecting current EoR power spectrum limits.

With the use of bispectrum phase, questions about the interpretation of its relationship to power spectrum have arisen. Here, we formulate simple steps to tie it back to physical units associated with a standard power spectrum.

Corresponding author: Nithyanandan Thyagarajan
t_nithyanandan@nrao.edu

The measured complex bispectrum is written as the product of the measured visibilities:

$$B^{\rm m}_{\nabla}(f) = |B^{\rm m}_{\nabla}(f)|\, e^{i\phi^{\rm m}_{\nabla}(f)} \tag{1}$$
$$= V^{\rm m}_{pq}(f)\, V^{\rm m}_{qr}(f)\, V^{\rm m}_{rp}(f) \tag{2}$$
$$= \left[V^{\rm F}_{pq}(f) + V^{\rm HI}_{pq}(f) + V^{\rm N}_{pq}(f)\right] \left[V^{\rm F}_{qr}(f) + V^{\rm HI}_{qr}(f) + V^{\rm N}_{qr}(f)\right] \left[V^{\rm F}_{rp}(f) + V^{\rm HI}_{rp}(f) + V^{\rm N}_{rp}(f)\right], \tag{3}$$

where, subscripts denote baselines formed from a triad of antennas denoted by p, q, and r. Superscripts denote the additive components of the visibilities – F for foregrounds, HI for the EoR HI signal, N for noise, and m for the measured quantity. $\phi^{\rm m}_{\nabla}$ is the measured bispectrum phase which can be written as the sum of the three interferometric phases measured by the baselines forming the triad:

$$\phi^{\rm m}_{\nabla}(f) = \phi^{\rm m}_{pq}(f) + \phi^{\rm m}_{qr}(f) + \phi^{\rm m}_{rp}(f) \tag{4}$$
$$= \left[\phi^{\rm F}_{pq}(f) + \phi^{\rm F}_{qr}(f) + \phi^{\rm F}_{rp}(f)\right] + \left[\delta\phi^{\rm HI}_{pq}(f) + \delta\phi^{\rm HI}_{qr}(f) + \delta\phi^{\rm HI}_{rp}(f)\right] + \left[\delta\phi^{\rm N}_{pq}(f) + \delta\phi^{\rm N}_{qr}(f) + \delta\phi^{\rm N}_{rp}(f)\right] \tag{5}$$
$$= \phi^{\rm F}_{\nabla}(f) + \delta\phi^{\rm HI}_{\nabla}(f) + \delta\phi^{\rm N}_{\nabla}(f), \tag{6}$$

where, $\phi^{\rm F}_{pq}(f)$ is the interferometric phase due to the foregrounds. $\delta\phi^{\rm HI}_{pq}(f)$ and $\delta\phi^{\rm N}_{pq}(f)$ are the fluctuations introduced by the EoR HI signal and the noise, respectively, on $\phi^{\rm F}_{pq}(f)$. The individual components in the bispectrum phase is related to the respective components in the interferometric phases as:

$$\phi^{\rm F}_{\nabla}(f) = \phi^{\rm F}_{pq}(f) + \phi^{\rm F}_{qr}(f) + \phi^{\rm F}_{rp}(f), \tag{7}$$
$$\delta\phi^{\rm HI}_{\nabla}(f) = \delta\phi^{\rm HI}_{pq}(f) + \delta\phi^{\rm HI}_{qr}(f) + \delta\phi^{\rm HI}_{rp}(f), \tag{8}$$
$$\delta\phi^{\rm N}_{\nabla}(f) = \delta\phi^{\rm N}_{pq}(f) + \delta\phi^{\rm N}_{qr}(f) + \delta\phi^{\rm N}_{rp}(f), \tag{9}$$
$$\phi^{\rm T}_{\nabla}(f) = \phi^{\rm F}_{\nabla}(f) + \delta\phi^{\rm HI}_{\nabla}(f), \tag{10}$$

where, $\phi^{\rm T}_{\nabla}(f)$ is a true sky structure-based quantity comprising of the bispectrum phase of the foregrounds and that from the fluctuations due to the EoR HI signal. From, equations 6 and 10, it can be shown that $\phi^{\rm m}_{\nabla}(f)$ is a measure of $\phi^{\rm T}_{\nabla}(f)$ corrupted only by fluctuations due to thermal noise in the measurement of visibilities that get propagated to $\phi^{\rm m}_{\nabla}(f)$, and is independent of antenna gains and their uncertainties. For convenience throughout (unless specified), we drop the explicit dependence on f.

In a foreground dominated case as is typical of low frequencies, $|V^{\rm HI}_{pq}|, |V^{\rm N}_{pq}| \ll |V^{\rm F}_{pq}|$. This implies that the amplitude of interferometric phase fluctuations, $|\delta\phi^{\rm HI}_{pq}| \approx |V^{\rm HI}_{pq}|/|V^{\rm F}_{pq}|$ and $\delta\phi^{\rm N}_{pq} \approx |V^{\rm N}_{pq}|/|V^{\rm F}_{pq}|$ are small and can be approximated as $|\delta\phi^{\rm HI}_{pq}|, |\delta\phi^{\rm N}_{pq}| \ll 1$. Therefore, $|\delta\phi^{\rm HI}_{\nabla}|, |\delta\phi^{\rm N}_{\nabla}| \ll 1$.

In order to relate the bispectrum phase to interferometric measurements, namely, complex visibilities and power spectrum, we take a simple approach while making use of approximations valid to the first order. Neglecting second and higher order terms in $V^{\rm HI}_{pq}$ and $V^{\rm N}_{pq}$ in Equation 3,

$$|B^{\rm m}_{\nabla}|\, e^{i\phi^{\rm m}_{\nabla}} \approx |B^{\rm F}_{\nabla}|\, e^{i\phi^{\rm m}_{\nabla}} \tag{11}$$
$$\begin{aligned} &\approx V^{\rm F}_{pq}\, V^{\rm F}_{qr}\, V^{\rm F}_{rp} \\ &\quad + V^{\rm F}_{pq}\, V^{\rm F}_{qr}\, V^{\rm HI}_{rp} + V^{\rm F}_{pq}\, V^{\rm F}_{rp}\, V^{\rm HI}_{qr} + V^{\rm F}_{qr}\, V^{\rm F}_{rp}\, V^{\rm HI}_{pq} \\ &\quad + V^{\rm F}_{pq}\, V^{\rm F}_{qr}\, V^{\rm N}_{rp} + V^{\rm F}_{pq}\, V^{\rm F}_{rp}\, V^{\rm N}_{qr} + V^{\rm F}_{qr}\, V^{\rm F}_{rp}\, V^{\rm N}_{pq} \\ &\quad + \text{higher order terms in } V^{\rm HI} \text{ and } V^{\rm N}. \end{aligned} \tag{12}$$

Then,

$$e^{i(\phi^{\rm F}_{\nabla} + \delta\phi^{\rm HI}_{\nabla} + \delta\phi^{\rm N}_{\nabla})} \approx e^{i\phi^{\rm F}_{\nabla}} \left[1 + \left(\frac{V^{\rm HI}_{pq}}{V^{\rm F}_{pq}} + \frac{V^{\rm HI}_{qr}}{V^{\rm F}_{qr}} + \frac{V^{\rm HI}_{rp}}{V^{\rm F}_{rp}}\right) + \left(\frac{V^{\rm N}_{pq}}{V^{\rm F}_{pq}} + \frac{V^{\rm N}_{qr}}{V^{\rm F}_{qr}} + \frac{V^{\rm N}_{rp}}{V^{\rm F}_{rp}}\right)\right] \tag{13}$$

Using a Taylor series expansion for small angles $\delta\phi^{\rm HI}_{\nabla}$ and $\delta\phi^{\rm N}_{\nabla}$,

$$e^{i(\phi^{\rm F}_{\nabla} + \delta\phi^{\rm HI}_{\nabla} + \delta\phi^{\rm N}_{\nabla})} \approx e^{i\phi^{\rm F}_{\nabla}} [1 + i(\delta\phi^{\rm HI}_{\nabla} + \delta\phi^{\rm N}_{\nabla})] \tag{14}$$

Identifying Equation 13 with Equation 14, it can be seen that

$$\delta\phi_{\nabla}^{\mathrm{HI}} = -i\left(\frac{V_{pq}^{\mathrm{HI}}}{V_{pq}^{\mathrm{F}}} + \frac{V_{qr}^{\mathrm{HI}}}{V_{qr}^{\mathrm{F}}} + \frac{V_{rp}^{\mathrm{HI}}}{V_{rp}^{\mathrm{F}}}\right), \tag{15}$$

$$\text{and,} \quad \delta\phi_{\nabla}^{\mathrm{N}} = -i\left(\frac{V_{pq}^{\mathrm{N}}}{V_{pq}^{\mathrm{F}}} + \frac{V_{qr}^{\mathrm{N}}}{V_{qr}^{\mathrm{F}}} + \frac{V_{rp}^{\mathrm{N}}}{V_{rp}^{\mathrm{F}}}\right). \tag{16}$$

Thus, in simple words the bispectrum phase fluctuations, $\delta\phi_{\nabla}^{\mathrm{HI}}$ and $\delta\phi_{\nabla}^{\mathrm{N}}$ are a measure of the HI line strength to foreground continuum ratio, and noise-to-foreground continuum ratio, respectively. If a model of the foreground visibilities is available, the EoR HI line strength can be estimated from this ratio.

Therefore, using HERA visibilities on these baselines after LST binning and averaging across repeating nights, we construct the quantity

$$\xi_{\nabla}(f) = |V_{\nabla}|\, e^{i\left(\phi_{\nabla}^{\mathrm{F}}(f) + \delta\phi_{\nabla}^{\mathrm{HI}}(f) + \delta\phi_{\nabla}^{\mathrm{N}}(f)\right)}. \tag{17}$$

The multiplication by $|V_{\nabla}|$ that is empirically representative of the effective foreground visibility amplitude from the triads converts the ratio to an effective flux density. Note that the explicit dependence on f has been re-introduced to emphasize that $|V_{\nabla}|$ is not a function of frequency but only provides an overall amplitude scaling that corresponds to the frequency band of interest centered at f_0. Combining equations 13 through 17, we can re-write $\xi(f)$ as:

$$\xi_{\nabla}(f) \sim V_{\mathrm{eff}}^{\mathrm{F}}(f) + V_{\mathrm{eff}}^{\mathrm{HI}}(f) + V_{\mathrm{eff}}^{\mathrm{N}}(f), \tag{18}$$

where,

$$V_{\mathrm{eff}}^{\mathrm{F}}(f) = e^{i\phi_{\nabla}^{\mathrm{F}}(f)}\, V_{\nabla}, \tag{19}$$

$$V_{\mathrm{eff}}^{\mathrm{HI}}(f) = i\,\delta\phi_{\nabla}^{\mathrm{HI}}(f)\, V_{\nabla}, \tag{20}$$

$$\text{and,} \quad V_{\mathrm{eff}}^{\mathrm{N}}(f) = i\,\delta\phi_{\nabla}^{\mathrm{N}}(f)\, V_{\nabla}. \tag{21}$$

Equation 18 falls in the familiar territory where the measured visibilities comprise of an additive combination of foregrounds, the cosmological HI signal from the EoR, and measurement noise. Whereas in traditional power spectrum approaches this is obtained by very precise calibration where the risk of introducing spectral features is high, we have arrived at effectively the same relation without any antenna-based calibration errors by bypassing such a calibration altogether.

The process of determining V_{∇} is empirical. We note that the variance due to HI and noise fluctuations is approximately the sum of the variances in the fluctuations in the individual interferometric phases. From equations 15 and 16, this can be expressed as:

$$\sigma_{\nabla}^{\mathrm{HI}} \simeq \left[\left(\frac{V_{pq}^{\mathrm{HI}}}{V_{pq}^{\mathrm{F}}}\right)^2 + \left(\frac{V_{qr}^{\mathrm{HI}}}{V_{qr}^{\mathrm{F}}}\right)^2 + \left(\frac{V_{rp}^{\mathrm{HI}}}{V_{rp}^{\mathrm{F}}}\right)^2\right]^{1/2}, \tag{22}$$

$$\text{and,} \quad \sigma_{\nabla}^{\mathrm{N}} \simeq \left[\left(\frac{V_{pq}^{\mathrm{N}}}{V_{pq}^{\mathrm{F}}}\right)^2 + \left(\frac{V_{qr}^{\mathrm{N}}}{V_{qr}^{\mathrm{F}}}\right)^2 + \left(\frac{V_{rp}^{\mathrm{N}}}{V_{rp}^{\mathrm{F}}}\right)^2\right]^{1/2}. \tag{23}$$

Assuming that the EoR signal strength and noise rms measured on each of the baselines forming the triad is similar, the fluctuations are inversely dependent on the foreground visibility measured on the respective baselines. The weakest visibility amplitude among the baselines in the triad will induce the maximum fluctuations which will dominate the overall fluctuation amplitude in the measured bispectrum phase. Therefore, we set

$$V_{\nabla}^{-2} = (V_{pq,f_0}^{\mathrm{M}})^{-2} + (V_{qr,f_0}^{\mathrm{M}})^{-2} + (V_{rp,f_0}^{\mathrm{M}})^{-2}, \tag{24}$$

where, V_{pq,f_0}^{M} denotes a reliable visibility model (obtained either through calibration or modeling) averaged over the frequency band of interest centered at $f = f_0$.

It must be highlighted that none of these empirical steps introduces any spectral structure other than that present in the original measurements. It may be argued that the use of V_{f_0} may leak some information about calibration uncertainties into the analysis, but since these are band-averaged and applied as a scalar factor to scale the bispectrum phase, it may introduce some uncertainty in the overall amplitude but will not impart additional spectral structure. Hence, the amplitude uncertainty, at this stage of the experiment, is definitely not required to be precise to the same level a regular power spectrum analysis that relies on precision calibration is required to be. In other words, if an overall amplitude uncertainty of 10% is introduced by the empirical determination of V_∇, the overall amplitude of the power spectrum will be uncertain only to the extent this 10% uncertainty is propagated to the power spectrum, and no new spectral structure that is not already present in data is introduced.

For obtaining the delay cross-power spectrum, we define the delay spectrum of $\xi_\nabla(f)$ as:

$$\Xi_\nabla(\tau) = \int \xi_\nabla(f)\, W(f)\, e^{i2\pi f\tau}\, df \tag{25}$$

and obtain the delay cross-power spectrum as:

$$P_\nabla(k_\parallel) \equiv \mathfrak{Re}\left\{\Xi_\nabla(\tau)\, \Xi^*_{\nabla'}(\tau)\right\} \left(\frac{\Delta D}{B^2_{\rm eff}}\right), \tag{26}$$

where, $B_{\rm eff}$ is the effective bandwidth centered on the frequency corresponding to redshift z, $\Delta D \equiv \Delta D(z)$ is the comoving depth along the line of sight at z corresponding to $B_{\rm eff}$, $k_\parallel \approx 2\pi\tau B_{\rm eff}/\Delta D$ is line-of-sight wavenumber, and $\mathfrak{Re}\{\cdot\}$ denotes the real part. In this memo, we use cosmological parameters from Planck Collaboration et al. (2016) with $H_0 = 100\,h$ km s^{-1} Mpc^{-1}. $P_\nabla(k_\parallel)$ is in units of Jy$^2\,h^{-1}$ Mpc. Modulo a couple of cosmological factors (Parsons et al. 2012), these are in the same units of a standard power spectrum. ∇ and ∇' could denote same or different measurements owing to differences in triads, LST, or night of observing. When $\Xi_\nabla(\tau) = \Xi_{\nabla'}(\tau)$, $P_\nabla(k_\parallel)$ reduces to delay auto-power spectrum. As already noted earlier, Equation 18 represents an equivalence between $\xi_\nabla(f)$ and visibilities. Therefore, $\mathrm{P}_\nabla(k_\parallel)$ in Equation 26 is equivalent to the standard power spectrum in the same units.

2. CURRENT STATE OF THE BISPECTRUM PHASE APPROACH

Figure 1 shows the current state of the power spectra obtained from 30 equilateral 29.2 m triads spanning $\sim$ 40 minutes of LST centered on the transit of Fornax A with 18 nights of observing in the HERA IDR2.1. These 18 nights of data have been split into two halves. In each of these halves, the bispectrum phases were averaged to 60s records, then coherently averaged at a given LST across days. The triads were not assumed to be redundant and were only averaged incoherently in delay cross-power spectrum. The delay cross-power spectrum was estimated by cross-multiplying the same LST and various pairs of "redundant" triads across two coherently averaged halves from 18 nights of observing. These cross-power spectra are then incoherently averaged over the different pairwise combinations of identical LST as well as both identical and non-identical triads.

We highlight the following:

1. **The main highlight** is that the dynamic range achieved at $|k_\parallel| \gtrsim 1\,h$ Mpc^{-1} is $\sim 10^{7.5}$–10^8 relative to the peak at $k_\parallel = 0\,h$ Mpc^{-1}. The presence of $\sim$ 50% negative values (solid circles show absolute value of the negative values), especially at $|k_\parallel| \gtrsim 1\,h$ Mpc^{-1}, implies that these results are still limited by noise and not systematics. The pairs of triads are denoted by "triad index" difference which is approximately a proxy for the physical distance between the triad pairs. The red curve corresponds to triad self-pairs while green, blue, and cyan curves indicate pairs of non-identical triads. The red curve can be considered as the conservative case where no loss of signal from the HI could have occurred because it is obtained from the cross-product between identical triads at the same LST in the two halves of observing nights. Noting that the dynamic range between $k_\parallel = 0\,h$ Mpc^{-1} and $|k_\parallel| \gtrsim 1\,h$ Mpc^{-1} remains relatively unchanged at $\sim 10^8$ and the peak at $k_\parallel = 0\,h$ Mpc^{-1} also remains unchanged, it indicates that there is no significant loss of the HI power even if the cross-power spectra from different but supposedly "redundant" triads are incoherently averaged. This strongly suggests that there may not be any relative signal loss whether triads are correlated and incoherently averaged with themselves or with others.

2. Power from the 150 m cable reflections is prominently seen at $\tau \approx 1\,\mu$s, which shows maximum coherency of the reflected standing waves at a level $\sim 10^5$ lower than the peak at $\tau = 0\,\mu$s when cross-power from identical triad

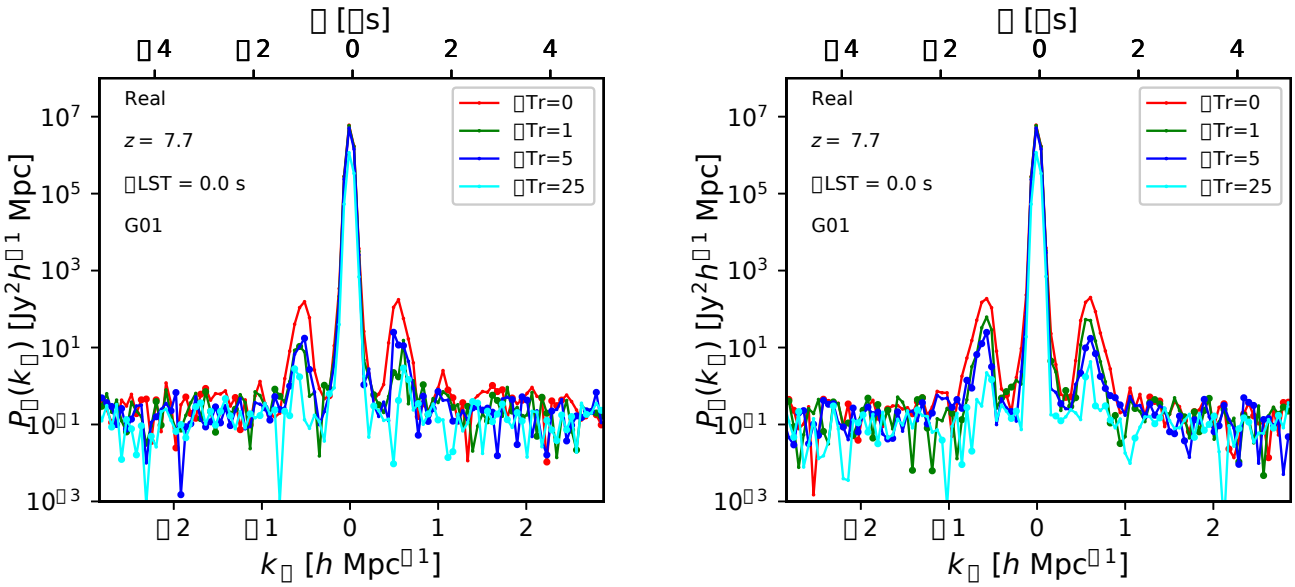

(a) XX polarization

(b) YY polarization

Figure 1. Delay cross-power spectrum, $P_\nabla(k_\parallel)$, of bispectrum phase of equilateral triads formed from 29.2 m baselines in two polarizations – XX (left) and YY (right), for a band centered around frequency corresponding to $z = 7.7$, and a total LST duration of ~ 40 minutes centered on the transit of Fornax A. $P_\nabla(k_\parallel)$ is in units of $\mathrm{Jy}^2\,h^{-1}$ Mpc, which is the same as for a standard power spectrum modulo a couple of cosmological factors. With 18 days of observing, the bispectrum phases are coherently averaged into 60 s bins of LST and two 9 night bins of the 18 observed nights. The cross-power spectrum is calculated by cross-multiplying the same LST and various pairs of "redundant" triads across two coherently averaged halves from 18 nights of observing. These cross-power spectra are then incoherently averaged over the different pairwise combinations of identical LST as well as both identical and non-identical triads. Red curves denote the incoherent averaging of the cross-power spectra over pairs of identical triads (differing in index by 0) across the two halves of the 18 nights observed. Green, blue, and cyan curves denote the same but incoherent averaging over non-identical triad pairs that differ in index by 1, 5, and 25, respectively. The solid circle symbols denote negative values in the cross-power spectra but only the absolute values are plotted. In most of the k-modes at $|k_\parallel| \gtrsim 1\,h$ Mpc^{-1}, the dynamic range relative to the peak is $\sim 10^{7.5}$–10^8. The double peak seen at $\tau \approx \pm 1\,\mu$s is probably due to reflections in the 150 m cables. This power from cable reflections is most prominent (at a factor of 10^5 lower than the peak at $\tau = 0\,\mu$s) for cross-power obtained from incoherent averaging of identical triads (red). The incoherent average over non-identical triads results in lowering the power in the cable reflection peak by a factor of 10 to 100 (factor of 10^6 to 10^7 lower than the main peak). The incoherent averaging of cross-power spectra of non-identical triads helps significantly in suppressing the power from the 150 m cable reflections.

pairs are incoherently averaged (red curve). This is because the standing waves from the reflections are expected to be most coherent (even across two halves of the 18 nights). If the incoherent average over non-identical triads (non-zero index difference, where index difference is assumed to be a proxy for the distance separating the triads) is examined, the standing waves are much less coherent which results in lowering the power in the cable reflection peak by a factor of 10 to 100 (factor of 10^6 to 10^7 lower than the main peak). Thus, an incoherent averaging using non-identical but supposedly redundant triads significantly mitigates this systematic but does not seem to result in loss of the cosmological signal.

3. At no stage in the analysis, has any new spectral structure been introduced.

4. It must also be emphasized that the units of the cross-power spectrum are equivalent to that of a usual power spectrum (though a couple of cosmological factors still need to be included in equation 26).

Similar figures were also obtained using the median statistic for coherent and incoherent averaging. These are shown in Figure 2. Qualitatively, no major differences are noted. HERA memos 54 and 55 go into the details of data inspection and data selection, including examining the effects of potential systematics and their impact on the power spectrum.

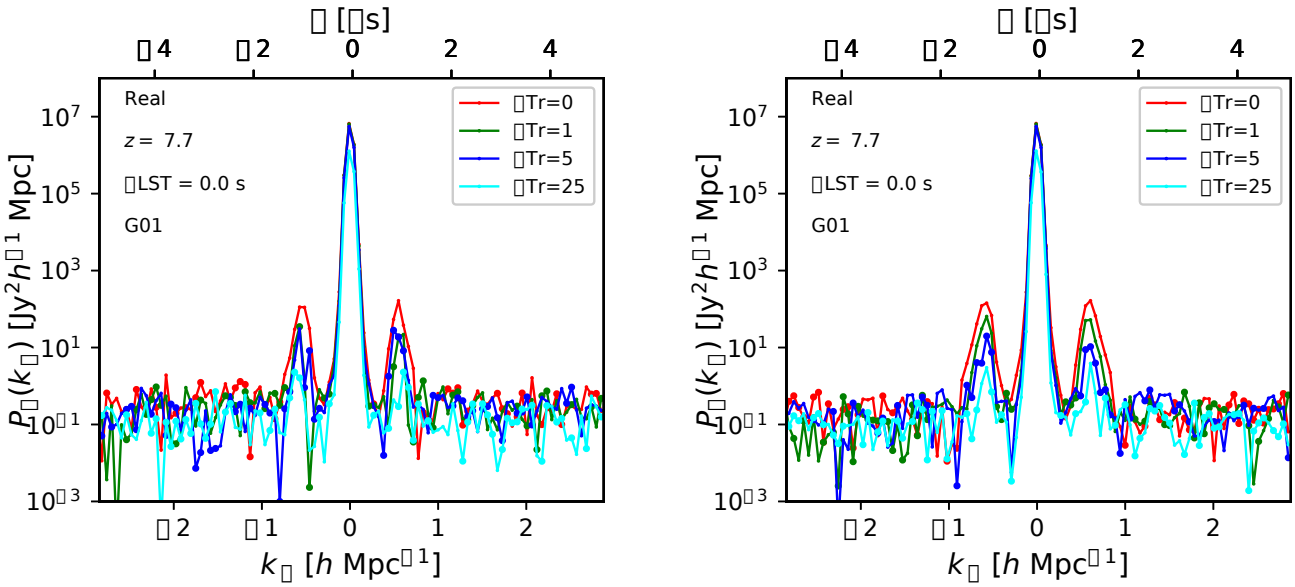

(a) XX polarization

(b) YY polarization

Figure 2. Same as Figure 1 but the coherent and incoherent reduction was done using the median statistic instead of the mean.

3. FUTURE PROSPECTS TO IMPROVE SENSITIVITY

There are many avenues being considered to improve the dynamic range further, the primary being using the 100 days from IDR3, and perhaps more. These include:

- Average the cross-power spectra from the two polarizations. This is expected to improve the dynamic range by a factor of $\sqrt{2}$.
- Average the cross-power spectra after appropriate weighting of all triad pairs including identical and non-identical ones (all triad index differences).
- Include larger LST intervals and there by increase sky coverage and further average the cross-power spectra obtained over longer times.
- Coherent averaging of bispectrum phase across more nights of observing can significantly improve the sensitivity to the EoR HI signal.
- Improvement in sensitivity can be obtained by incoherent averaging of neighboring LST intervals (up until the EoR HI signal turns incoherent).
- Any avenue for further coherent averaging (such as from triads behaving redundantly) or more observing nights while repeating the same LST range will improve the sensitivity.

4. MODELING

Figure 3 shows a simulated model of the bispectrum phase expected from different foreground components and a fiducial EoR HI signal (Greig & Mesinger 2017) at a generic location on the sky reproduced from Thyagarajan et al. (2018).

Figure 4 (reproduced from Thyagarajan et al. (2018)) shows the corresponding delay power spectra at three frequency bands centered on 125 MHz, 150 MHz, and 175 MHz. Although not in the same units as in equation 26 or Figure 1, since we are only drawing inferences about relative ratios and dynamic ranges, the conclusions drawn here remain valid even if different units are used. It is seen that the power spectrum of bispectrum phase depends on the foreground and EoR models, and is very sensitive to the ratio of EoR signal strength to the foreground continuum. The contributions

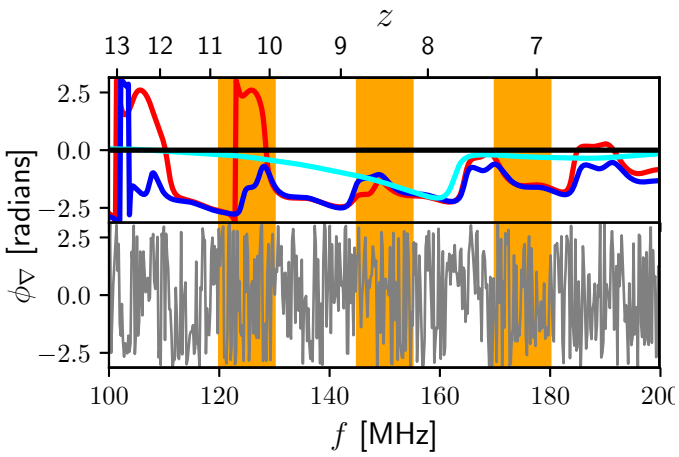

Figure 3. [Reproduced from Thyagarajan et al. (2018)] Simulated bispectrum phase spectra of individual components in the sky model – single point source (black) with $\phi_\nabla = 0$, compact sources (cyan), diffuse foregrounds (blue), diffuse and compact components combined (red), and the EoR HI fluctuations (gray) – for a 14.6 m equilateral triad. The HI component is highly fluctuating relative to the foregrounds. The phase wrap discontinuities at $\phi_\nabla = \pm\pi$ are not of a physical origin. The orange sub-bands centered at 125 MHz (left), 150 MHz (middle), and 175 MHz (right) are representative of different redshift bands analyzed in the simulation.

from the EoR HI fluctuations, $\delta\phi_\nabla^{\rm HI}$, are detected as they dominate over $\phi_\nabla^{\rm F}+\delta\phi_\nabla^{\rm N}$ at $|k_\parallel| \gtrsim 0.5\,h$ Mpc^{-1} in the 150 MHz and 175 MHz sub-bands. As the EoR HI signal strength increases (ten-fold in $\langle(\delta T_{\rm b}^{\rm HI}(z))^2\rangle^{1/2}$), the separation in $P_\nabla(k_\parallel)$ also increases at $|k_\parallel| \gtrsim 0.5\,h$ Mpc^{-1} (~ 100 times), most clearly in the 150 MHz and 175 MHz sub-bands.

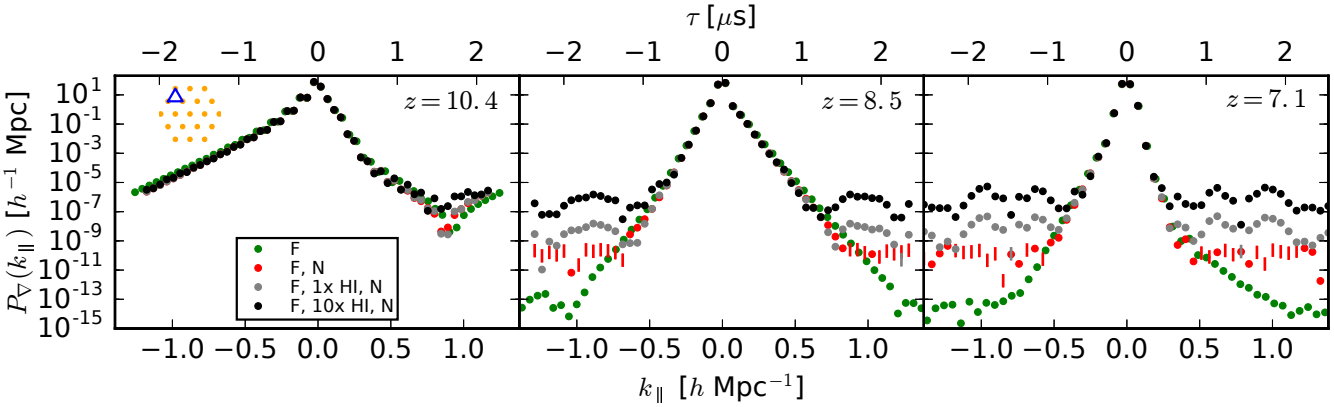

Figure 4. [Reproduced from Thyagarajan et al. (2018)] Delay power spectra of simulated bispectrum phases in sub-bands centered at 125 MHz (left), 150 MHz (middle), and 175 MHz (right) that include contributions from foregrounds, EoR signal, and noise. The corresponding redshifts are listed in each panel. The 14.6 m equilateral triad used is highlighted on a HERA-19 layout on the top left. Green curves show only the foreground contribution ($\phi_\nabla^{\rm m} = \phi_\nabla^{\rm F}$). The anisotropic foreground model employed Thyagarajan et al. (2015) results in the asymmetry around $k_\parallel = 0\,h^{-1}$ Mpc. The red curves show the effect of including noise fluctuations ($\phi_\nabla^{\rm m} = \phi_\nabla^{\rm F} + \delta\phi_\nabla^{\rm N}$), after averaging $N_{\rm m} \sim 10^6$ measurements. The gray curves apply when fluctuations from the EoR HI signal are included, $\phi_\nabla^{\rm m} = \phi_\nabla^{\rm F} + \delta\phi_\nabla^{\rm HI} + \delta\phi_\nabla^{\rm N}$. The black curves are identical to the gray ones except the EoR HI signal is 10 times brighter. The dot and vertical markers denote positive and negative values respectively. The latter results from the removal of noise bias by using cross-power spectra (Eq. 26). The EoR HI contribution is significantly detected at $|k_\parallel| \gtrsim 0.5\,h$ Mpc^{-1} at $z \approx 8.5$ and $z \approx 7.1$. At $z \approx 10.4$, the EoR contribution is inseparable from foregrounds because the EoR signal is weaker (see power spectrum of FAINT GALAXIES model at $k = 0.5$ Mpc^{-1} in Fig. 2 of Greig & Mesinger (2017)) while the foregrounds are brighter. The detection significance depends on the strength of EoR HI signal relative to the foregrounds. A 10-fold increase in EoR intensity shows a $\sim$ 100-fold increase in $P_\nabla(k_\parallel)$ at $|k_\parallel| \gtrsim 0.5\,h$ Mpc^{-1} at $z \approx 8.5$ and $z \approx 7.1$, indicating its sensitive dependence on he line-to-continuum ratio. Therefore, this detection measures the line-to-continuum ratio, from which the EoR HI brightness temperature fluctuations, $\langle(\delta T_{\rm b}^{\rm HI}(z))^2\rangle$, can be inferred using a reliable foreground model.

However, such a clear separation is not observed in the 125 MHz band. The redshift evolution of separability in $P_\nabla(k_\parallel)$ depends on relative strengths of the foreground and the EoR HI signal. In the 175 MHz sub-band ($z \approx 7.1$), relative to the 150 MHz sub-band ($z \approx 8.5$), $\langle(\delta T_{\rm b}^{\rm HI}(z))^2\rangle$ is weaker (see FAINT GALAXIES model at $k = 0.5$ Mpc^{-1} in Fig. 2 of Greig & Mesinger (2017)) but the foreground synchrotron temperature is also fainter roughly by the same factor. Therefore, the separability of EoR HI in $P_\nabla(k_\parallel)$ is roughly similar in the two sub-bands. However, in the 125 MHz sub-band ($z \approx 10.4$), $\langle(\delta T_{\rm b}^{\rm HI}(z))^2\rangle$ in the fiducial EoR model is fainter but the foregrounds are brighter, thereby significantly decreasing the spectral contrast between foregrounds and the EoR signal. Hence, a clear separability is not seen at $z \approx 10.4$.

Another noticeable aspect is that the shape of the foreground contribution to the power spectrum (inner 'core' of the power spectrum), appears to vary depending on the frequency band of interest and the structure of the foregrounds in these frequency bands. This is due to a combination of the foregrounds, and the antenna power pattern varying as a function of frequency, which drives the frequency structure of the foregrounds seen in the closure phase spectra (Fig. 3). For instance, in the low frequency band, the continuum has substantial structure in the closure spectrum (Fig 3), and the resulting power spectrum has a broad core (Fig 4). At the high frequency band, the closure phase structure with frequency is relatively smooth and of lower amplitude, and the power spectrum shows a narrow core.

In the HERA IDR2.1 data around Fornax A transit, the power in the central core ($|k_\parallel| \lesssim 0.3\,h$ Mpc^{-1}), is similar in the two bands analyzed (see the associated memos 54 and 55), and very narrow, essentially unresolved in k-space. This results from the fact that the Fornax field is dominated by the Fornax A radio source, which is essentially a point source at the resolution of these short baselines. The point source drives the closure phase spectra close to zero, with only gradual fluctions of at most $\pm 20^o$. Since this structure does not vary significantly across the bands, the shape of the power spectrum in the inner $k_\parallel$ modes also does not differ significantly.

Remarkably, a dynamic range of $\sim 10^8$ as seen in the data begins to be at the level where an EoR HI slightly stronger than a fiducial model appears to be separable in some of the frequency bands as seen in the previous modeling effort.

A parallel modeling effort is being undertaken to verify the specific behaviour of the foregrounds in the Fornax A field, a fiducial EoR HI signal, and the noise components in the power spectrum results and to confirm these findings. This is not only necessary to calibrate the scaling of the amplitudes of these various components that are at the moment only empirically determined, but will also address the uncertainties in the power spectrum estimates. Finally, it will make a direct comparison with the other power spectrum approaches straightforward.

5. SUMMARY

We have known that the bispectrum phase depends sensitively on the ratio of the EoR HI line to the foreground continuum. In this memo, we have shown that bispectrum phase can be "flux calibrated" by a foreground model for the visibilities to obtain relations very similar to that of the standard power spectrum approach. Therefore, the power spectrum results from the bispectrum approach are comparable in amplitude and units to that of a standard power spectrum. After an initial selection of HERA IDR2.1 data that now includes ~ 30 equilateral-shaped triads with 29.2 m baselines on each side, ~ 40 minutes of LST around Fornax A, and 18 nights of observing, we are able to achieve a noise-limited dynamic range of $\sim 10^{7.5}$–10^8 between the foreground-dominated peak at $k_\parallel = 0\,h$ Mpc^{-1} and the power spectrum tail where noise (and eventually the EoR HI signal) is expected to dominate at $k_\parallel \gtrsim 1\,h$ Mpc^{-1}. It must be emphasized that no potentially new spectral spectral structure or EoR HI signal loss has been introduced at any stage in this processing. The noise-limitedness indicates that there is definite scope for further improvement with more data. We report noticing power from the cable reflections at $\tau \approx \pm 1\,\mu$s but can be mitigated to a dynamic range of $\sim 10^7$ via cross-power spectra obtained between different subsets of the data such as different triads that should be similar, adjacent LST bins, and different halves of the 18 nights of observing. Modeling efforts are underway to understand in detail the behaviour of the foregrounds, EoR HI, and noise components in the observed bispectrum phase power spectrum and establish the precise numerical connection to a standard power spectrum. Based on previous modeling results, the current data appears to be very interesting where the dynamic range of 10^8 achieved begins to be at the level an EoR HI signal slightly stronger than fiducial levels can start becoming distinguishable from the foreground and noise levels in the power spectrum. This needs to be vigorously tested and confirmed.

REFERENCES

Carilli, C., & Nikolic, B. 2017, A closer look at closure, HERA Project Memorandum 35, HERA Collaboration. http://reionization.org/wp-content/uploads/2013/03/HERA19.Comm4_.pdf

Carilli, C. L., Nikolic, B., Thyagarayan, N., & Gale-Sides, K. 2018, Radio Science, 53, 845

Carilli, C. L., & Sims, P. 2016, ArXiv e-prints, arXiv:1607.00147

Greig, B., & Mesinger, A. 2017, MNRAS, 472, 2651

Kent, J., Carilli, C., Nikolic, B., Thyagarajan, N., & Beardsley, A. 2018, Closure Diagnostics, HERA Project Memorandum 48, HERA Collaboration. http://reionization.org/wp-content/uploads/2013/03/hera-memo-048-kent-closure-3.pdf

Parsons, A., Pober, J., McQuinn, M., Jacobs, D., & Aguirre, J. 2012, ApJ, 753, 81

Planck Collaboration, Ade, P. A. R., Aghanim, N., et al. 2016, A&A, 594, A13

Thyagarajan, N., Carilli, C. L., & Nikolic, B. 2018, Physical Review Letters, 120, 251301

Thyagarajan, N., Jacobs, D. C., Bowman, J. D., et al. 2015, ApJ, 804, 14